

A Efficient Multimodal Framework for Large Scale Emotion Recognition by Fusing Music and Electrodermal Activity Signals

Guanghao Yin, Shouqian Sun, Dian Yu and Kejun Zhang*, *Member, IEEE*

Abstract—Considerable attention has been paid for physiological signal-based emotion recognition in field of affective computing. For the reliability and user friendly acquisition, Electrodermal Activity (EDA) has great advantage in practical applications. However, the EDA-based emotion recognition with hundreds of subjects still lacks effective solution. In this paper, our work makes an attempt to fuse the subject individual EDA features and the external evoked music features. And we propose an end-to-end multimodal framework, the 1-dimensional residual temporal and channel attention network (RTCAN-1D). For EDA features, the novel convex optimization-based EDA (CvxEDA) method is applied to decompose EDA signals into pahsic and tonic signals for mining the dynamic and steady features. The channel-temporal attention mechanism for EDA-based emotion recognition is firstly involved to improve the temporal- and channel-wise representation. For music features, we process the music signal with the open source toolkit openSMILE to obtain external feature vectors. The individual emotion features from EDA signals and external emotion benchmarks from music significantly are fused in the classifying layers. We have conducted systematic comparisons with single EDA, single music and EDA-music fused inputs on three multimodal datasets (PMEmo, DEAP, AMIGOS) for 2-classes valance/arousal emotion recognition. Our proposed RTCAN-1D outperforms the existing state-of-the-art models, which also validate that our work provides a reliable and efficient solution for large scale emotion recognition. Our code has been released at <https://github.com/guanghaoyin/RTCAN-1D>.

Index Terms—Multimodal Fusion, Large Scale Emotion Recognition, Attention Mechanism.

1 INTRODUCTION

THE ability of emotion recognition is a significant hallmark of intelligent Human-Computer Interaction (HCI). Empowering computers to discern human emotions better would make them perform the appropriate actions. In recent two decades, both the research groups and industries have aroused great interest that explore to enhance user experience with algorithms [1]. With the advancement of sensor-based Internet of Things (IoT) technology, emotion recognition is on unceasing demand by a wide range of applications such as mental healthcare [2], driving monitor [3], wearable devices [4], etc.

Human emotions are generally described as a group of affective states evoking as responses to stimulations from external environments or interpersonal events [5]. According to the behavioral researches, emotions are typically described as the set of discrete basic categories [6]. They can also be represented in the continuous space [7], [8], which can quantitative describe the abstract emotion state. The valence-arousal space is one of the common emotion discrete space, where the valence reflects the value of the positive to negative state and the arousal measures the

active to calm degree [9], [10]. For the advantage of conducting the Self-Assessment Manikins (SAM), most of the popular open-source multimodal emotion datasets applied the valence-arousal annotations like DEAP dataset with 32 subjects [11], AMIGOS dataset with 40 subjects [12], the current largest PMEmo dataset with 457 subjects [13], or etc.

In general, the data source of emotion recognition can be categorized into (1) peripheral physical signals such as facial expression [14], speech [15]; (2) physiological signals including Electroencephalography (EEG), Electrodermal Activity (EDA), Electrocardiogram (ECG), or etc. The first method has great advancement of data collection. However, it cant guarantee the recognition reliability because human can consciously control body languages to hide their personal emotion like speech tone or facial expression. Compared with the former, using physiological signals can overcome this drawback. The physiological signals are reacted from the autonomic and somatic nervous systems (ANS and SNS). They are largely involuntarily activated and cannot be triggered by any conscious or intentional control [16]. Thus, the physiological signal-based method provides an avenue to recognize affect changes which are less obvious to perceive visually [16].

For physiological signals based emotion recognition, two broad methods exist: (1) the traditional well-designed classifiers with hand-crafted features; (2) the deep learning models with auto feature extraction. According to previous studies, the wide range of statistical features has been explored to seek the predictive potency for emotion classification including time domain, frequency domain, and time-frequency domain features [17], [18], [19], [20], [21], [22].

- Guanghao Yin, Shouqian Sun, Dian Yu are with the Key Laboratory of Design Intelligence and Digital Creativity of Zhejiang Province, Zhejiang University, Hangzhou 310027.

Kejun Zhang is with the Key Laboratory of Design Intelligence and Digital Creativity of Zhejiang Province, Zhejiang University, Hangzhou 310027, and also with Alibaba-Zhejiang University Joint Research Institute of Frontier Technologies.

E-mail: {ygh_zju, ssq, yudian329, zhangkejun}@zju.edu.cn

However, the hand-crafted features based methods suffer limitations in the following aspects. First, the design of hand-crafted feature strongly depends on prior knowledge of statistics and physiology in the small scale data. Second, researchers should take more and more effective hand-crafted features into account for better performance. It is a great challenge for their feature selection method. Although, Shukla [17] has provided a systematic exploration of feature selection method, it cannot guarantee the robustness with large scale complicated physiological signals. Recently, the effectiveness of deep learning models have been proven in tackling emotion recognition [23], [24], [25], [26]. Moreover, the end-to-end DNN model can directly learn discriminative features from data. Therefore, in order to involve less prior knowledge and explore the general solution for large scale emotion recognition, we choose the end-to-end deep learning model.

To the best of our knowledge, there are few systematic works of the EDA-based user independent emotion recognition for large scale data. Compared with other physiological signals, the acquisition of EDA can be conveniently accomplished with the finger or wrist transducer. It can be easily completed by intelligent wearable devices like smartwatches, wisebraves. The research of EDA-based emotion recognition can be faster put into practical applications like emotion monitor, music liking recommendation, or etc. Considering the great significance of scientific value and practicability, the goal of our research is to contribute in the general end-to-end solution for EDA-based user independent emotion recognition.

Establishing the relationship between emotion state and the physiological signals with large scale subjects is a challenging problem, which is also important for the validity, reliability, and generalizability application. On the early stage of physiological signal-based emotion recognition, researchers focused on the user dependent task. There exists excellent user dependent systems to obtain more than 90% accuracy for one subject multiple emotions recognition task [27], [28]. When extending the subject from one to group, the accuracy of user independent models decreased greatly [16] because of the individual specificity. Specifically, we have conducted subject incremental classification with single EDA in Section 5.2.1. In relatively small scale datasets with dozens of subjects, such as DEAP (32 subjects), AMIGOS (40 subjects) and 1/10 PMemo datasets (46 subjects), the models can build the accurate relationships between EDA and emotion central states. However, the subjects' individual specificity determines the more subjects involve, the less consistent the features of the same class are. When we gradually increase the subject number of PMemo dataset to the maximum 457, the representation power of models with single EDA input can not converge. To solve this problem, we consider the multimodal fusion. Music is commonly utilized mediums in laboratory environment because they are effective to modulate subjects mood [29], [30]. Therefore, we choose the music signal from large scale PMemo dataset as the external constraints for supervised learning. Fusing the music features can also overcome the defect that the EDA signal is relevant for arousal classification [17], [31].

In this paper, we propose RTCAN-1D, a novel end-to-end 1D residual temporal and channel attention network

for emotion recognition in valence-arousal dimension. We directly apply 1D residual block to build the EDA residual feature extraction (RFE). In order to provide sufficient useful messages from 1-channel EDA, we apply the convex optimization-based EDA method [32] to decompose EDA into phasic, tonic components and feed the 3 channel mixed signals (origin, phasic and tonic) into RTCAN-1D. Then, we involve the attention mechanism: (1) the signal channel attention module (SCA) to reweight the features of 3-mixed signal channels; (2) the residual non-local temporal attention module (RNTA) to explore the temporal correlations of EDA features. To the best of our knowledge, our model is the first attempt to involve attention mechanism to process physiological signals. The EDA decomposition, two attention blocks and residual feature extraction form the residual temporal and channel attention group (RTCAG) to get the EDA feature vectors. Moreover, the external music features are extracted with the open source toolkit openSMILE. Finally, The classifying layers fuse individual emotion features from EDA signals and external emotion benchmarks from music to predict the emotion state. The overall structure of our model is illustrated in Fig 1 and Fig 2.

We compare our model with previous researches on three popular datasets: the effectiveness of RTCAG with single EDA input is evaluated on the small scale DEAP and AMIGOS datasets; the effectiveness of RTCAN-1D with multimodal input is evaluated on large scale PMemo dataset. For fair comparison with the state-of-the-art methods, our proposed model was conducted for binary classification in valence and arousal.

In summary, the contributions of our paper are represented as follows:

- We propose an end-to-end multimodal framework RTCAN-1D for user independent emotion recognition.
- The fusion of dynamic and steady features from phasic and tonic EDA components significantly improve the performance of our model.
- The fusion of individual specificity from EDA and external static benchmark from music provides a great solution for large scale emotion recognition.
- The effectiveness of attention mechanism is firstly proved to capture the channel-wise correlations and long-distance temporal informations of EDA signals.

Our paper is organized as follows. Section 2 introduces literatures and reviews of related works. In Section 3, our proposed model is explained in detail. Experimental validations and result analysis are described along with the implementation details in Section 4. The slights and discussions are expressed in Section 5. Finally, we conclude this paper in Section 6 by summarizing the attributions and future prospects.

2 RELATED WORK

2.1 Emotion Representation

As we focus on emotion recognition, the emotions should be represented quantitatively. Psychologists model the emotion in two mainstreams: (1) dividing the emotion into discrete classes; (2) using the multi-dimensional emotion space.

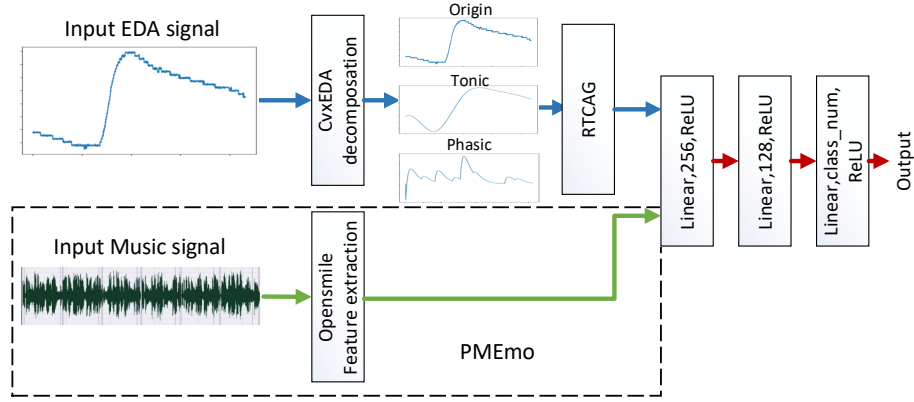


Fig. 1. **Overall architecture of the proposed method.** Music signals are only applied for PMemo dataset, the music-evoked large scale EDA dataset with hundreds of subjects. For other three datasets, the model is only fed with single EDA input. For fair comparison with previous works, the class number is set to 2 in DEAP, AMIGOS and PMemo. The structure of residual temporal and channel attention group (RTCAG) is illustrated in Fig. 2.

The discrete emotion representation uses several keywords to describe the emotion rates. Plutchik [33] proposed a wheel model that includes eight basic emotions. In his model, the stronger emotions are in the center while the weaker emotions are surrounded. More complex emotions can be formed by the mix of basic ones. Then, Damasio [34] categorised the emotions as primary (deriving from innate fast and responsive behaviour) or secondary (deriving from cognitive thoughts). Izard [35] extended to 10 basic emotions. However, the discrete description is unsuitable to analyze complex emotions, because some mixed emotions can not be precisely expressed in words.

The second mainstreams presented a certain degree of specific emotional level in the multi-dimensional emotion space. A first attempt was proposed by Wundt [36], where emotions were described in a pleasure-displeasure, excitement-inhibition, tension-relaxation 3D space. In 1979, Russell [9] postulated a two-dimensional model, spanned by the axes valence and arousal. The valence reflects the value of the positive or negative state and the arousal measures the active or calm degree [37]. Now, the V/A model becomes one of the most frequently employed model because it can be easily assessed using the Self-Assessment Manikins (SAM) [38]. The three affective datasets used in this paper are all measured by V/A space.

2.2 Multimodal Fusion for Emotion Recognition

The multimodal fusion has great advantage to rich the complementary information from different modalities [39], which has a very broad range of successes, including emotion recognition [38], multi-sensor management [40], human computer interaction [41].

To improve the robustness and performance of emotion recognition, previous researchers combine different physiological signals [16], [27], [42], including ECG, RSP, EMG, EDA and EEG, because the fused signals contain more implicit informations with the different sampling rate and more channels. But collecting multi-signals requires many conductive electrodes placed along the subject's scalp. The user-unfriendly acquisition limits practical applications. Therefore, some works added external media messages,

which have great relationship with human emotion. Kim *et al.* [43] systematically present the robust emotion recognition fusing the speech and biosignals. Liu *et al.* [44] combined the evoked video and EEG signals to predict subject emotion state. Koelstra *et al.* [45] combined the facial expression with EEG signals. And Thammasan *et al.* [46] fused the EEG and musical features. There is no effective exploration for the fusion of EDA and music signals, especially with large scale subjects. Hence, our paper focuses on this issue.

2.3 EDA Processing

The EDA signal is widely used in psychology or physiology field. The approaches to process EDA signal include Bayesian Statistics [17], [47], dictionary learning [48], [49] and decomposition [50]. We focus on the end-to-end general solution. Hence, the complex processing is inappropriate. Therefore, we choose to decompose the EDA. The frequently used measurement of EDA is skin conductance (SC), which is comprised of tonic, phasic components [51]. The tonic phenomena (t) reflects slow drifts of the baseline level and spontaneous fluctuations in SC. The phasic phenomena (r) is generally a short-time rapid fluctuation and reflects the response to external stimulation [51]. For realistic tasks, the measurement noise of equipments is also taken into consideration.

In the past decades, there have been several mathematical solutions for EDA decomposition associated with stimulus. Referring to Alexander *et al.* [50], the well-known assumption is that the SC equals to the convolution between discrete bursting episodes of sudomotor nerve activity (SMNA) and biexponential impulse response function (IRF):

$$SC = SMNA * IRF. \quad (1)$$

There exists some methods for EDA decomposition. Discrete Deconvolution Analysis (DDA) [52] claims the non-negativity of the driver and maximal compactness of the impulses to decompose EDA by means of non-negative deconvolution. Continuous Decomposition Analysis (CDA) [53] improves DDA with the IRF called Bateman function to conduct continuous decomposition. Convex Optimization-Based EDA Method (CvxEDA) [32] models the phasic, tonic,

noise components and applies convex optimization to solve the maximum a posteriori (MAP) problem. CvxEDA provides a novel method to decompose EDA without preprocessing steps and heuristic solutions [54].

2.4 Attention Mechanism

In human proprioceptive systems, attention generally provides a guidance to focus on the most informative components of an input [55]. Recently, attention models improves the performance of deep neural networks for various tasks, ranging from video classification [56] to language translation [57]. Pei *et al.* [58] proposed a temporal attention module to detect salient parts of the sequence while ignoring irrelevant ones in sequence classification. Wang *et al.* [56] proposed a portable non-local module for spatical attention to capture long-range dependencies in video classification. Hu *et al.* [55] proposed SENet to incorporate channel-wise relationships to achieve significant improvement for image classification.

To the best of authors' knowledge, the attention mechanism has not been applied in physiological-based emotion recognition. As the mixed 3-channel input is sequential, each channel may contribute differently to the final prediction in different temporal range. In this work, we exploit an efficient channel-wise and temporal attention mechanism according to 3-channel mixed EDA characteristics.

3 PROPOSED METHOD

3.1 Network Framework

The great success of CNN frameworks depends on 2D convolution in signal processing and image domain [59], [60], [61]. Our previous work [62] in EDA-based emotion recognition with the PMemo dataset [13] also conducted 2D convolution. However, it is a detour to transform 1D signal to 2D matrix just for finetuning pretrained 2D CNN backbones. Accordingly, we directly use 1D residual CNN framework to process EDA signals in this work.

The overall architecture of the proposed method is illustrated in Fig. 1. Let the vector $X_T = \{x_1, x_2, \dots, x_t\}$ be the input EDA sequence with t points. $Y_{class} = \{y_1, \dots, y_c\}$ denotes the groundtruth for c -classes task. If the emotion state belongs to the i^{th} class, $y_i = 1$ and $y_j = 0$ for $j \neq i$. Our goal is to establish the relationships between input EDA and emotion state, specifically decreasing the distance between groundtruth label Y_{class} and predicted result \hat{Y}_{class} .

Firstly, we conduct CvxEDA decomposition and the 1-channel EDA signal is expanded to mixed 3-channel signal $X_{TC} = \{(x_{11}, x_{12}, x_{13}), \dots, (x_{t1}, x_{t2}, x_{t3})\}$. As shown in Fig. 2, the expanded signal is subsequently fed into residual temporal and channel attention group (RTCAG). The EDA feature vector is extracted by three parts: shallow feature extraction, attention module and residual feature extraction.

One convolutional layer extracts shallow feature F_{SF} as:

$$F_{SF} = H_{SF}(X_{TC}), \quad (2)$$

where $H_{SF}(\cdot)$ denotes convolution and batch-normalization operation. Then, the attention module reweights the shallow

feature and focuses on more useful parts in temporal and channel-wise dimensions as:

$$F_A = H_A(F_{SF}), \quad (3)$$

where F_A is rearranged feature and $H_A(\cdot)$ is the attention module respectively. To mining the discriminative representations, we design the residual feature extraction ($H_{RF}(\cdot)$) with the backbone of ResNet-18 [61] to output a EDA feature vector (F_{EF}):

$$F_{EF} = H_{RF}(F_A). \quad (4)$$

It should be emphasized that there exists other excellent CNN architectures such as VGG [63], GoogLeNet [64] or DenseNet [65] to mine deep feature, but a comparison of different CNN frameworks is not the focus of our research. To be specific, for dozens of people involved EDA dataset, the subjects' specificity is not so complicated that the RTCAN-1D can handle the single EDA input, which means $F_{FF} = F_{EF}$. For large scale PMemo dataset with hundreds of subjects, we fuse the EDA feature with external static media feature (F_{MF}). Under this circumstances, the full feature vector is the concatenation of EDA feature and media feature:

$$F_{FF} = Cat(F_{EF}, F_{MF}). \quad (5)$$

Finally, the series linear layers ($H_{CF}(\cdot)$) are fed with the full feature vector (F_{FF}) and output the classifying vector (\hat{Y}_{class}) with the Softmax function

$$\hat{Y}_{class} = Softmax(H_{CF}(F_{FF})). \quad (6)$$

3.2 CvxEDA Decomposition

Before extracting meaningful features from EDA, we apply CvxEDA decomposition for feature augmentation. In this subsection, the mathematical deduction of CvxEDA will be briefly introduced. As explained in Section 2.3, the observed signal (y) is composed of three N-long column vectors: the phasic (r) and tonic (t) signal plus the noise component (ε):

$$y = t + r + \varepsilon. \quad (7)$$

This equation can be rewritten as:

$$y = MA^{-1}p + B\lambda + Cd + \varepsilon. \quad (8)$$

where $r = MA^{-1}p$ and $t = B\lambda + Cd$. For denoising in the process of solving optimization problem, the prior probability of noise term is discarded. Then, with the transcendental knowledge of physiology and taking logarithmic transtorm, the MAP problem can be rewritten as a standard Quadratic-Programming (QP) convex form and can be solved efficiently using many available solvers (see more details in [32]):

$$\begin{aligned} \min & \frac{1}{2} \|MA^{-1}p + B\lambda + Cd - y\|_2^2 + \alpha \|MA^{-1}p\|_1 + \frac{\gamma}{2} \|\lambda\|_2^2 \\ \text{subject to} & MA^{-1}p \geq 0. \end{aligned}$$

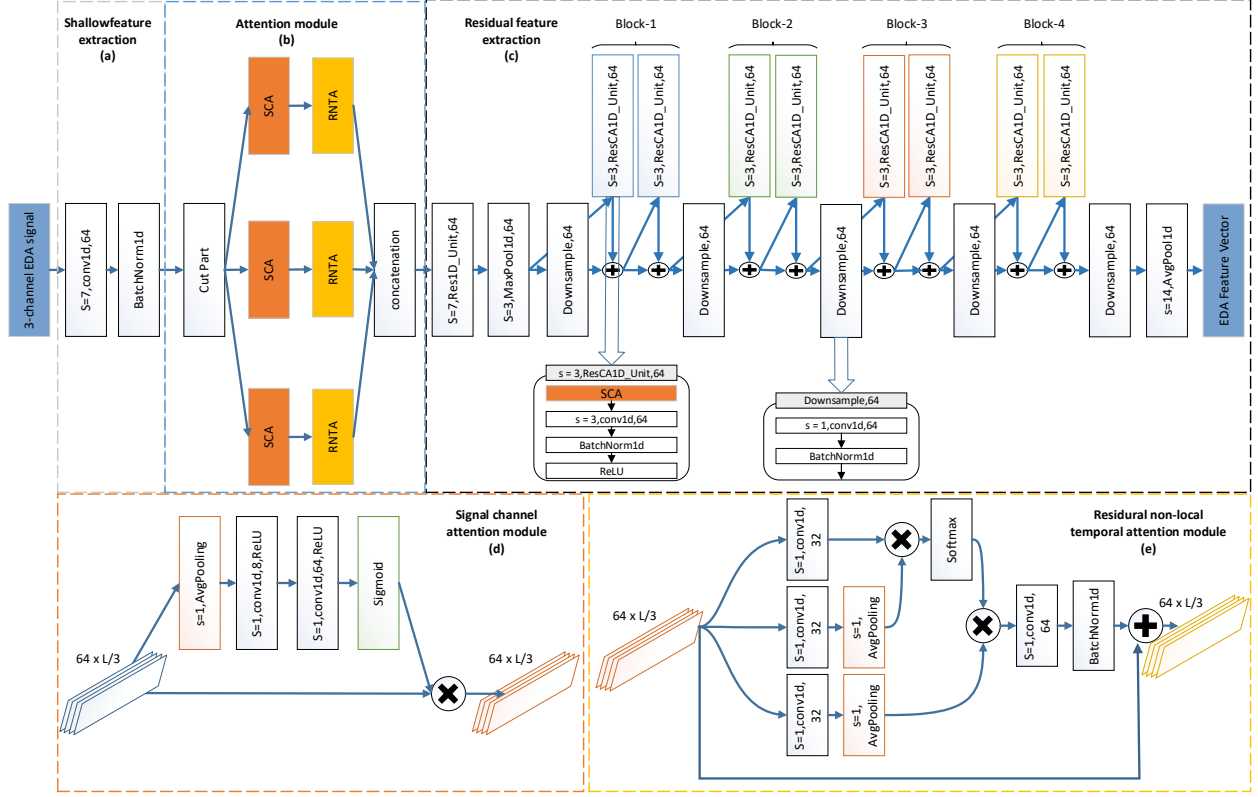


Fig. 2. **The structure of the residual temporal and channel attention group** consists of (a) shallow feature extraction, (b) attention module and (c) residual feature extraction (RFE). Specifically, attention module contains (d) signal channel attention module (SCA) and (e) residual non-local temporal attention module (RNTA). It should be emphasized that the three blocks of The SCA and RTNA are the same one respectively which is recurrently used to reduce the modules' parameters.

3.3 Residual Temporal and Channel Attention Group

Now we show our residual temporal and channel attention group (RTCAG) (seen in Fig. 2). After the shallow feature extraction, the feature map is processed with the series structures of signal channel attention module (SCA), residual non-local temporal attention module (RNTA) and residual feature extraction (RFE) to output a EDA feature vector. The purpose of attention mechanism is to adaptively reweight the shallow feature for more useful messages in channel and temporal dimensions. Hence, the SCA and RNTA are plugged before RFE. To reduce the computational expense and mine the inter-channel correlation between different time phase, we split the shallow features in temporal-level and feed the clips into SCA and RNTA in order.

3.3.1 Signal Channel Attention Module

For multi-channel input, different channels make different contributions to the certain target. We involve channel-wise attention mechanism to exploit the inter-channel relationship and adaptively reweights them. It recently has been a hotspot in various researches like image captioning [66], image classification [67] or object detection [55]. By achieving great performance and robust to noisy inputs, channel-wise attention mechanism has been proven to be mobility and portability for different tasks. However, traditional attention module is limited by the unacceptable computational burden especially with large feature maps. Therefore, we consider to clip the long-temporal shallow

feature to smaller groups and recursively feed them into the module. Referring to various channel-wise attention module, our SCA is adapted from the simplest structure of Squeeze-and-Excitation Block in [55] and replaces the convolution with 1D operation to fit signal inputs (see in Fig. 2(d)). As mentioned before, the clipping operation benefits for both the efficiency of SCA and RNTA. But the number of clipping parts is considerable because an inappropriate division leads to the large size for each clips and the detailed division will cause the gradient and optimal issues for the SCA. Referring to [37], the EDA signal evoked from stimulations passes through a procedure of the latency, rise time, half recovery time. Although these intervals are not homogeneous in time, the physiological knowledge guides us to roughly divide the shallow feature to 3 parts in sequence dimension: $F_{SF} = [F_{SF_1}, F_{SF_2}, F_{SF_3}]$, where $F_{SF} \in R^{C \times L}$ and $F_{SF_1}, F_{SF_2}, F_{SF_3} \in R^{C \times L/3}$.

We firstly aggregate the temporal information from the clipped feature with the average-pooling operation to get the temporal average-pooled features $F_{avg}^{L/3}$. Then the descriptor is forwarded to a multi-layer perceptron (MLP) with only one hidden layer. In order to reduce parameter overhead, the channel of average-pooled features through the hidden layer W_0 is decreased by the reduction ratio r to $R^{C/r \times L/3}$, then recovered by the latter layer W_1 . The sigmoid activation function generates the normalized channel attention weight $W_R \in R^{C \times L/3}$ between 0 to 1. Finally, the original shallow feature is reweight by the multiplication with the

channel attention weight. Overall, the reweighted channel-wise feature is computed as :

$$\begin{aligned} F_{CA_i} &= \text{Sigmoid}(\text{MLP}(\text{AvgPool}(F_{SF}))) * F_{SF} \\ &= \text{Sigmoid}(W_1(W_0(F_{avr}^{L/3}))) * F_{SF}, \end{aligned} \quad (9)$$

where $i = 1, 2, 3$ and $F_{CA} = [F_{CA_1}, F_{CA_2}, F_{CA_3}]$ is forwarded to the RNTA to mine temporal-range dependencies.

3.3.2 Residual Non-local Temporal Attention Module

Non-local operation is firstly proposed as a neighborhood filtering algorithm in image domain [68]. It can involve the long-range position contribution to the filtered response of a certain position and control the contribution under the guidance of appearance similarity. At the advantage of capturing long-range relationships, the non-local neural network has been validated effective in video classification, object detection, instance segmentation and keypoint detection [56]. The great generality and portability motivates us to apply non-local operation in psychological signal-based emotion recognition.

However, as described in Section 3.3.1, traditional attention module will multiply the computational complexity for large size features. Therefore, the RNTA module performs piecewise non-local operation. It takes the three parts of clipping features from the SCA as the inputs. Similar to the SCA, the RNTA is also trained recursively to reduce the model complexity.

Referring to [56], [68], the generic non-local operation in deep neural networks can be defined as:

$$\hat{x}_i = \frac{1}{c(x)} \sum f(x_i, x_j) g(x_j), \quad (10)$$

where x represents the input feature map, i is the target index of an output position in time sequence and j is the index of all possible locations which contribute to the filtered response \hat{x}_i . The output \hat{x}_i has the same size of input x . Specifically, the function $g(\cdot)$ changes the representation of input feature. The function $f(\cdot)$ computes the scale between i and all j . The function $c(\cdot)$ is the normalization function before the output. The formulations of function $c(\cdot)$, $g(\cdot)$ and $f(\cdot)$ depends on the specific network structure.

In our module (seen in Fig. 2(e)), we set 1D convolution operation and a average-pooling operation with kernel of size 1 to conduct linear embedding as:

$$g(x_j) = \text{AvgPool}(W_g x_j). \quad (11)$$

For pairwise function $f(\cdot)$, there exists various formulations to the relationship between long-range indexes like Embedded Gaussian, Concatenation or etc. Wang *et al.* [56] has validated that the performance of non-local operation is insensitive to the instantiations of function $f(\cdot)$ and $g(\cdot)$. Hence, we choose the commonly used Embedded Gaussian function [57] and define $f(\cdot)$ as:

$$f(x_i, x_j) = e^{\theta(x_i)^T \phi(x_j)}, \quad (12)$$

where $\theta(\cdot)$ and $\phi(\cdot)$ are the convolutional layer. Adapted from [56], we set $c(x) = \sum_{\forall j} f(x_i, x_j)$, then $\frac{1}{c(x)} f(x_i, x_j)$ equals to the softmax operation. So non-local operation is computed as:

$$\hat{x} = \text{softmax}(x^T W_\theta^T \text{AvgPool}(W_\phi x)) \text{AvgPool}(W_g x). \quad (13)$$

Finally, we combine the non-local operation and the residual connection to get the output of attention module (F_{A_i}):

$$F_{A_i} = F_{RNTA_i} = W_w F_{NL_i} + F_{CA_i}, \quad (14)$$

where F_{CA_i} is the clipped input from the SCA module, F_{NL_i} is calculated by Eq.(13), W_w denotes the 1D convolution operation followed with the batch normalization and $F_A = [F_{A_1}, F_{A_2}, F_{A_3}]$ is the reweighted output of our attention module.

3.3.3 Residual Feature Extraction

The structure of EDA feature extraction module is shown in Fig.2(c). Our residual feature extraction (RFE) applies the ResNet-18 [61] as the backbone. Considering the training efficiency, the dimension of signal sequences and the complexity of physiological signals which are less obvious to perceive relationship with labels visually, we make two modifications: (1) replacing all the 2D convolutional layer to 1D convolutional operation for directly mining features from 1D signal; (2) simplifying the residual basic block that only conducts stacking 1D convolutional layer, batch normalization layer and ReLU non-linear activation function for one time; (3) adding a signal channel attention layers at before the 1D convolution to mine the channel relationships between the deep features. Finally, the module extracts the EDA feature vector F_{EF} from attention reweighted features F_A . Specifically, we found that in small scale dataset, the SCA of residual block would increase the model complexity to cause the overfitting. Therefore, we removed the SCA in RTCAG for DEAP and AMIGOS datasets.

3.3.4 Multimodal Fusion Classification

Compared with image or speech recognition tasks, the complicated shapes of physiological curves determine that the physiological signal based emotion recognition is a tough problem. Its not intuitive to perceive the relationship between the emotion state and the input curve. Moreover, personal specificity determines the intricate difference of nonemotional individual contexts between persons [27], especially in datasets with large scale subjects.

Our experiments in Table 9 shows that the proposed model performs well with the single EDA input in DEAP and AMIGOS. But the result is unsatisfactory in PMemo because of the dataset difference. The PMemo involves 10 more times subjects which can not help the model to converge but challenge the generalization ability. Moreover, the EDA signals of PMemo contains less information with lower sampling frequency (50HZ). In order to solve those problems, We conduct multimodal fusion by adding some static benchmarks, which are accessible and have great relationship with emotion state.

Specifically for our previous PMemo dataset, music is the external medium to raise emotion states with affection involvement which can be conveniently used as the prior benchmark. We attempt to combine prior features from external stimulation and individual specific features from physiological signal. In our previous work [13], music feature extraction has been accomplished in PMemo dataset with a open source toolkit openSMILE. As Fig. 1 illustrates, the EDA feature vector and music feature vector are concatenated and forwarded to the multi-linear classification

layers. The classifier consists of three linear layers followed with a ReLU function. The output channels are 256, 128 and the class number respectively. Finally, the output vector is normalized by the softmax function and the maximum one is chosen as the predicted result.

4 DATASET ANALYSES

As the performance of classifier is relevant to the data distribution. In this section, we will conduct pre-experiments to analyze the characteristics of three multimodal affective datasets, including DEAP [11], AMIGOS [12] and PMemo [13], which can explain the experiment results in Section 5.2.

4.1 Datasets Introduction

DEAP. The database for emotion analysis using physiological signals (DEAP) is one of the most explored datasets for analysis of affective states. The 32 participants (19-37 years, 50% females) separately watched 40 one-minute long videos. Meanwhile, the central nervous signal EEG and peripheral nervous signals including electromyogram (EMG), electrooculogram (EOG), skin temperature (TMP), galvanic skin response (GSR), blood volume pulse (BVP), and respiration (RSP) were recorded at a 512Hz sampling rate and later down-sampled to 256Hz. Finally, the subjects performed the assessment of float subjective-ratings on arousal, valence, liking and dominance scales. The EDA data in this paper is downloaded from the dataset server named "data_preprocessed_python.zip", which has been downsampled to 128Hz and segmented into 60 second trials. The 3 second pre-trial baseline has been removed.

AMIGOS. The dataset for affect, personality and mood research on individuals and groups (AMIGOS) consists of the short videos and long videos experiments: (1) the 16 clips of short videos were watched by 40 subjects; (2) the 37 subjects were separated to watch 4 long videos where 17 subjects performed in individual setting and 5 groups of 4 people did in group setting. During two experiments, physiological signals (EEG, ECG, GSR) were captured, where GSR signals are recorded at 128HZ. Each participant rated each video in valence, arousal, dominance, familiarity and linking, and selected from 7 basic emotions. In our paper, we downloaded the preprocessed and segmented version from the "data_preprocessed_matlab.zip".

PMemo. The popular music dataset with emotional annotations (PMemo) is our previous work [13]. To the best of our knowledge, it is the current largest emotion recognition dataset with EDA and music signal. It contains 7962 pieces of EDA signals from 457 subjects. The chorus excerpts clipped from 794 pop songs are collected as the emotion elicitation. After relaxing procedure, the subjects listened to music and the EDA signals were collected from subjects finger at 50-HZ sampling rate. Meanwhile, the subject conducted dynamic V/A discrete annotation and static V/A discrete annotation for each chorus. In this work, we utilize static annotations to represent emotion state and fuse the EDA and music signal for large scale emotion recognition.

4.2 Annotation Recreation

The annotations from above datasets are ranged from 1 to 9. As mentioned before, we attempt to conduct 2-class

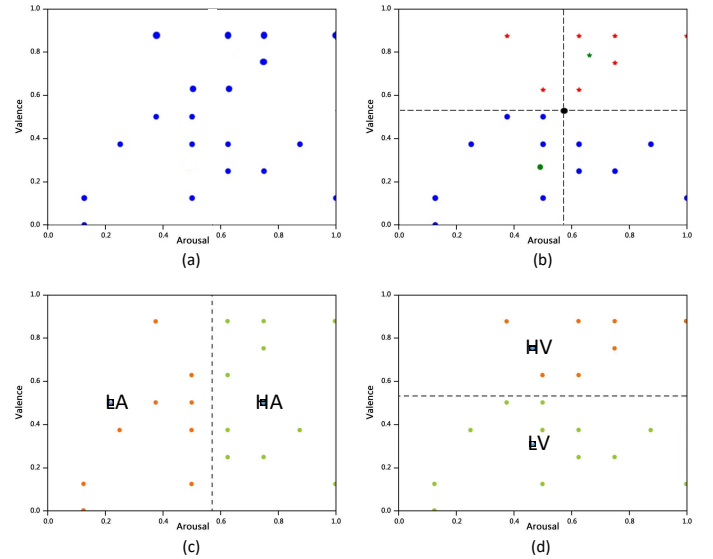


Fig. 3. Visualization of the binary emotion label generation from one subject (ID:10031). (a) The annotation collection from a subject in the V/A emotional space; (b) The k-means clustering to calculate two cluster centers and their midpoint; (c) The high and low arousal state separated by threshold; (d) The high and low valence state separated by threshold.

TABLE 1
The statistics of binary relabeled annotations in valence and arousal in three datasets

Dataset	V/A	Num of high class	Num of low class
PMemo	Arousal	4520 (58.8%)	3170 (41.2%)
	Valence	4436 (57.7%)	3254 (42.3%)
DEAP	Arousal	680 (53.1%)	600 (46.9%)
	Valence	647 (50.5%)	633 (49.5%)
AMIGOS	Arousal	443 (56.2%)	345 (43.3%)
	Valence	394 (50.0%)	394 (50%)

recognition in DEAP, AMIGOS and PMemo for the fair comparison with previous works. Therefore, the annotations should be relabeled to the appropriate classes.

Focusing on user independent emotion recognition with large scale subjects, we should pay more attention to the personal specificity. The different emotion thresholds result in that the same V/A score totally maps to the opposite emotion state between different subjects. It should be noted we involved the subject threshold just for generating proper subject-specific emotional classes. The user-independent model should not focus on on a specific individual user but deal with greatly varying individual differences. But it doesn't mean that we can ignore the subject-specificity when recreating the binary label from the original dispersed annotation. When mapping the 1-9 annotations to the binary classes, previous work [69] simply discretized the annotations into low (≤ 5) and high (≥ 5) V/A states. The reference [63] points out that since the subjective ratings also possess the non-stationarity and subject-specificity, the fixed threshold may not be suitable for all individual preferences. If we attempt to validate the generalization of our work in large scale data, personal threshold generating subject-specific emotional classes are essential. Specifically, inspired by the strategy in [69], [70] for binary classification, we

TABLE 2

The statistics of correlation between the annotated arousal and valence scores in three datasets.

Dataset	Correlation	P-Value
AMIGOS	$r = 0.56$ [17]	$p \leq .001$ [17]
DEAP	$r = 0.15$	$p \leq .001$
PMemo	$r = 0.52$	$p \leq .001$

calculate the subject’s emotion threshold with discrete annotations as the example of one subject (Subject-ID: 10031 from PMemo) shown in Fig. 3. The statistics of each class after label recreation is shown in Table 1. It validates the relabeled processing will not cause imbalanced label distribution.

4.3 Annotation Correlation

Previous works point out the EDA signal is relevant for arousal classification [17], [31]. However, the results reported by [12], [17], [71] show that the classification performance for the valence and arousal dimensions does not diverge considerably. Shukla *et al.* [17] reveals that the subject preferences of V/A annotation scores greatly influence the gap of V/A performance. In the specific dataset, the subject tends to annotate the valence score associated with arousal score, where the correlations of V/A scores is high. To systematically analyze the experiment results in Section 5.2, we should firstly analyze the annotation correlations in DEAP, AMIGOS and PMemo datasets. The statistics are listed in Table 2. It is clear that there are significant and quite high correlations between the annotated arousal and valence scores of AMIGOS and PMemo, where the valence annotations in those two datasets have been influenced by arousal annotations. For DEAP dataset, the subject has no preference to annotate the valence scores associated with arousal annotations. The characteristics of annotation can explain that our model delivers the accurate valence recognition with AMIGOS and PMemo datasets, and the performance of valence variable is much lower than arousal one in DEAP dataset.

4.4 Rough Recognition Baselines with SVM

The EDA distribution is greatly influenced by the subject specificity, which also influences the recognition performance in different dataset. To roughly evaluate the classification baselines in those three datasets, we should conduct the preliminary assessment by pre-experiments. Referring to [12], the SVM classifier with linear kernel were separately trained and tested on three datasets. As we attempted to roughly analyze the quality of EDA distribution, the mixed origin + phasic + tonic vectors were directly fed into the SVM classifier without feature extraction. We referred to [12] and set the regularization parameter C of the linear SVM to 0.25. The results are shown in Fig. 3. It can be seen that the recognition results of AMIGOS and DEAP dataset are similar. As the EDA feature was not extracted, the performance for V/A variables in DEAP did not diverge considerably. The various subject specificity and lower sampling frequency could explain why the SVM performed worse with PMemo dataset. The PMemo involved 457 subjects,

TABLE 3

Mean accuracies and F1-scores of SVM classifier for valence and arousal recognition in AMIGOS, DEAP and PMemo datasets.

Dataset	Valence		Arousal	
	Accuracy	F1-score	Accuracy	F1-score
AMIGOS	54.10%	57.28%	55.54%	57.20%
DEAP	53.63%	55.21%	55.68%	56.75%
PMemo	51.90%	54.42%	52.37%	54.88%

10 times larger than AMIGOS and DEAP. Our previous work [62] reported the Pearson Correlation coefficients between the EDA and V/A label were less than 0.06. When the inner class features are not consistent, more data from large scale subjects can not help the model to converge but challenge the generalization ability of the model. Moreover, we found the EDA signals of PMemo were downsampled with the 50HZ, which contained much less information than AMIGOS and DEAP at 128HZ.

5 EXPERIMENTS

In this section, we systematically conduct multimodal analyses with single EDA, single music and multimodal inputs in DEAP [11], AMIGOS [12] and PMemo [13] datasets. Specifically, we conduct subject incremental experiments to prove the individual specificity of PMemo greatly influence single EDA recognition. Moreover, we carry out the ablation study to present the effects of different components. The comparisons with previous solutions prove that our proposed multimodal framework can efficiently solve those problems. More details are presented as follows.

5.1 Training Settings

For PMemo dataset, the weights of the whole RTCAN-1D were initialized from the Gaussian distribution $N(0, 0.01)$. Then, the RTCAN-1D are initialized with the PMemo-trained parameters for the small scale DEAP and AMIGOS datasets. We trained our model with Cross-entropy loss and empirically selected the size of mini-batches as 256. The Stochastic Gradient Descent (SGD) was applied as the optimizer. Moreover, we set the initial learning rate to 0.001, which was decreased by 0.9 at every 15 epochs.

The proposed model was evaluated with 10-fold cross validation. The dataset was partitioned into 10 disjoint subsets with subject-independent scenarios [62], [72]. At each fold, one subset was set to the test data and the rest were used for training. Repeated 10 times, all the subsets were tested and the average metrics of all the 10 folds were calculated as the results. The performance of binary classification is evaluated with average accuracy and F1-score (the harmonic mean of precision and recall).

Before fed into deep neural network, the EDA and music signals will be preprocessed. Processed by CvxEDA, EDA signal was split to tonic, phasic components. The signal denoising could also be accomplished by convex optimization. The z-score normalization were conducted for three EDA and music signals. Moreover, we just used EDA signals after 3-second because annotators need some preliminary to evoke their emotion [73]. For input alignment, linear interpolation was also conducted to rescale EDA inputs.

TABLE 4
The comparison of different signal input in DEAP, AMIGOS and PMemo dataset.

Method	Dataset	Subject	Input signal	Valence		Arousal	
				Ave-accuracy	F1-Score	Ave-accuracy	F1-Score
RTCAG	DEAP	32	EDA	73.21%	77.37%	81.05%	83.10%
RTCAG	AMIGOS	40	EDA	74.13%	72.29%	77.36%	76.46%
RTCAG	PMemo-10%	46	EDA	71.22%	70.40%	72.61%	71.53%
RTCAG	PMemo-40%	128	EDA	65.43%	64.52%	65.60%	64.37%
RTCAG	PMemo-70%	319	EDA	63.82%	63.07%	64.79%	65.22%
RTCAG	PMemo	457	EDA	63.61%	62.47%	64.05%	64.82%
SVM [62]	PMemo	457	Music	70.43%	75.32%	71.49%	76.36%
RTCAN-1D	PMemo	457	EDA + Music	77.30%	80.94%	82.51%	85.62%

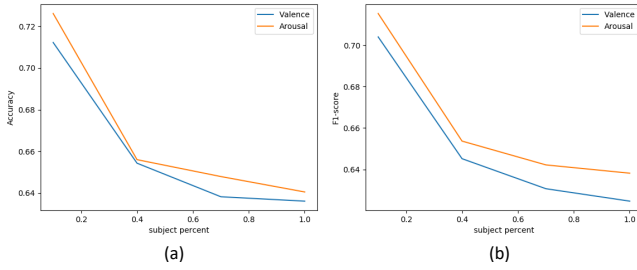


Fig. 4. The subject incremental results for valence and arousal dimensions in PMemo dataset. (a) Recognition accuracies; (b) F1-scores. It can be seen when the involved subjects increase to hundreds, the recognition results decrease drastically.

5.2 Multimodal Analyses

5.2.1 Single EDA Recogniton

To prove the effectiveness of the proposed multimodal framework, we should first prove that our RTCAG can extract useful EDA features. Therefore, we conduct single EDA recognition in three popular datasets, including DEAP, AMIGOS and PMemo. After being pre-processed, the composed 3-channel signals were fed into RTCAG and the series liner layers classified the EDA feature vectors.

The results in DEAP, AMIGOS and PMemo are listed on the 1st, 2nd and 6th rows of Table 4. It is clear that our model has accomplished accurate recognition in DEAP and AMIGOS, which proves the EDA feature extraction of RTCAG are excellent. Moreover, because of the annotation correlations, the results for V/A dimensions in AMIGOS and PMemo are relatively close and the performance in DEAP diverges considerably, which is aligned with the dataset characteristics in Section 4.3.

As we have described in Section 4, the larger scale subject and lower sampling frequency of PMemo will limit the recognition performance. To validate our assumption, we conduct a subject incremental experiment. The subjects from PMemo are gradually increased from 10% to 40%, 70% and 100%. Keeping the same training settings, the results are shown on the 3rd row to 6th row of Table 4 and illustrated in Fig 4. We can make some analyses: (1) Although there is a slightly better performance for arousal, the recognition performance for the two variables in four subject scales does not diverge considerably, which is aligned with the high annotation correlation of PMemo dataset as we have described in Section 4.3. (2) When the number of subjects (PMemo-10%) is similar to DEAP and AMIGOS, the recognition accuracies of RTCAG are lower but also competitive (more than 70%),

because the 50HZ EDA signals of PMemo contain less informations than 128HZ EDA signals of DEAP and AMIGOS. (3) When the involved subjects increase to hundreds, the recognition results decrease drastically. Different from the image or speech recognition task, the physiological signals have various curves, which has no consistent inner-class features. More individual specificity can not help the model to converge but challenge the generalization ability of the model. The lower results in large scale PMemo motivate us to involve complementary information by multimodal fusion.

5.2.2 Single Music Recogniton

For single music recognition, we directly used the result (SVM + Music) in our previous work [62]. The results are presented on the 7th row of Table 4. We can make some analyses: (1) Compared with single EDA input, the performance with single music input get improved for valence recognition, because the EDA is less relevant to the valance state [17], [31] but the music has strong relationship with subjects valence/arousal moods [29], [30]. It show be noted that the music feature method can not be regarded as the solution for user independent emotion recognition, because using the single music features can not recognize the emotion state of a specific person precisely. (2) For single music features, if considering subject specificity, the same music might lead to completely opposite emotion state which means the same music input maps to label 0 and 1 with different subject, such as the valence annotations of subject-ID 100179 and subject-ID 100184 with music-ID 1. Therefore, we add the music feature as the static emotion benchmark to help the convergence of our RTCAN-1D.

5.2.3 Fusing Music and EDA Recogniton

As subsection 3.3.4 indicates, our model fuses the emotion benchmarks from music stimulation and individual specific features from EDA signal in PMemo dataset. As shown on the last row of Table 4, the proposed model with multi-feature fusion achieves the best performance. For single EDA recognition, our model perform well in DEAP and AMIGOS, which proved the RTCAG can efficiently extract EDA features. But the end-to-end model performed unsatisfactorily in PMemo dataset because of the low sampling frequency and large scale individual specificity. The 7962 pieces of 3-channel EDA signals from 457 participants in PMemo dataset contained less informations and were more complex that the RTCAN-1D could not converge enough to classify them. For single music recognition, the classifier

TABLE 5

Comparison results with different signal inputs in PMemo dataset.

V/A	Input	Ave-accuracy	F1-Score	Precision	Recall
V	origin	67.75%	70.14%	74.26%	66.45%
	tonic	70.42%	76.58%	79.28%	74.05%
	phasic	72.35%	74.87%	81.17%	69.48%
	mixed	77.30%	80.94%	83.54%	78.49%
A	origin	75.49%	77.60%	80.86%	74.59%
	tonic	78.58%	82.35%	81.35%	82.78%
	phasic	79.17%	81.13%	81.95%	80.33%
	mixed	82.51%	85.62%	88.56%	82.86%

could not recognize the individual specificity because the music feature had no relationships with specific human. The significant improvement of RTCAN-1D validates that the fusion of external static features from music and individual specific features from EDA is an effective solution for large scale emotion recognition.

5.3 Ablation Analyses

To avoid the less-effective experiment repetition, we carry out the ablation study in the largest PMemo dataset.

5.3.1 Effects of CvxEDA Decomposition

In our previous work [62], a regression pre-experiment had validated that the decomposed phasic and tonic components were correlated with the recognition targets. After using CvxEDA, the RMSEs and correlation coefficients of phasic and tonic were higher than the EDA baseline [13] (see more details in [62]). Therefore, we were motivated to apply cvxEDA decomposition. For analysing the role of each signal and explaining why we chose the mixed 3-channel signal as input, retaining the music features, we respectively fed RTCAN with four types of EDA input, including origin, tonic, phasic and mixed signal. The results of different EDA components are listed in Table 5.

As results show in Table 5, we can make some analyses: (1) The RTCAN-1D with original signals gets the lowest accuracy due to the limited messages and the noise interference in raw data. (2) Between three types of single input, the model with tonic is steadiest and gets good F1-Score. The tonic reflects slow drifts of SCL, so it can provide the most stable message of EDA trends. (3) The model with phasic signals gets good accuracy because the phasic contains the dynamic activity to provide more short-term specific messages which has great correlation with final prediction. But the phasic is so intricate that the model with phasic signals also gets less steady performance with lower F1-Score. (4) The 3-channel signal leads to the best performance for the fusion of dynamic emotion feature from phasic and steady emotion feature from tonic. (5) Expanding the signal channels from 1 to 3 can explicitly utilize the representation ability of the attention mechanism. It may not be obvious for user dependent method or small scale dataset [26]. But for large scale user independent emotion recognition, the CvxEDA can really help the CNN model converge easier.

5.3.2 Res-block Configuration

As Fig. 1 and Fig. 2 illustrate, the residual feature extraction (RFE) is the principal part of the whole RTCAN-1D while the attention module, shallow feature extraction

TABLE 6

Trade-off between performance and the depth at each level of the residual block in PMemo dataset.

V/A	Depth	Channel	Ave-accuracy	F1-Score
V	1	[64,64,64,64]	77.30%	80.94%
	1	[64,128,256,512]	74.29%	78.37%
	2	[64,64,64,64]	72.70%	76.55%
	2	[64,128,256,512]	72.04%	74.95%
A	1	[64,64,64,64]	82.51%	85.62%
	1	[64,128,256,512]	78.84%	80.67%
	2	[64,64,64,64]	74.41%	75.02%
	2	[64,128,256,512]	72.90%	74.33%

and linear classifier are designed with the simplest structures. Therefore, the structure of RFE is the major determinants of computing cost. As explained in Section 3.3.3, we apply the Resnet-18 as the backbone and replace all 2D convolution operation with 1D version. Keeping the basic backbone of Resnet, the key problem addresses in the depth of res-block (the stacking 1D convolutional layer, batch normalization and ReLU) and the number of internal channels. The original settings of ResNet-18 are $d = 2$ and $c = [64, 128, 256, 512]$. We design the res-block with different configurations. The trade-offs between each structures are shown in Table 6.

In practice, we find the simplest structure achieves the best performance. By using deeper convolutional layer and more internal channels, the performance of RTCAN-1D get drop-off and the network can be easily overfitting, which is more obvious in smaller scale DEAP and AMIGOS datasets. In general, deeper network leads to better representation performance at the expense of space and time cost. However, when the inner class features are not consistent and the number of training data scale is not large enough, such as millions images for image recognition [74], the complicated structure is harmful for EDA feature extraction. It is much clear in Table 6. Therefore, we applied the simplest structure $d = 1$ and $c = [64, 64, 64, 64]$ for our res-block.

5.3.3 Effects of Attention Module

The proposed RTCAN-1D consists of the basic feature extraction model and attention modules. As explained before, simply designing deeper residual feature extraction network can not improve the representation ability. Therefore, we involve the attention mechanism which has achieved great success and proven to be portability in various tasks. There are two main components of our attention module: (1) signal channel attention module (SCA) mines the inter-channel relationship and rearranges the importance between different channels of shallow features; (2) residual non-local temporal attention module (RNTA) contributes the long-range position to the filtered features and reweight the input by capturing the relationships between long-time signal clips. To validate the effectiveness of combining method of SCA and RNTA, we compared 4 variants of model: the basic model without any attention module, the additive SCA model, the additive RTNA model and the final proposed RTCAN-1D.

Experimental results with different attention modules are shown in Table 8. *Base* refers to the basic model which only contains the ResNet backbone and multi-linear layers

TABLE 7

The arrangement method of attention submodules in PMEmo dataset. *Base* represents the rest of RTCAN-1D apart from attention module.

V/A	Arrangement	Ave-accuracy	F1-Score
V	Base + SCA + RTNA	77.30%	80.94%
	Base + RTNA + SCA	74.31%	77.42%
	Base + RTNA-SCA in parallel	74.10%	76.93%
A	Base + SCA + RTNA	82.51%	85.62%
	Base + RTNA + SCA	81.72%	84.46%
	Base + RTNA-SCA in parallel	80.21%	83.55%

TABLE 8

Comparison of different attention modules in PMEmo dataset.

Model	Base	Basic	R_a	R_b	R_c
	SCA	✓	✓	✓	✓
	RTNA			✓	✓
Valence	Ave-accuracy	74.60%	74.78%	74.93%	77.30%
	F1-score	78.33%	78.79%	78.99%	80.94%
Arousal	Ave-accuracy	75.82%	79.70%	80.11%	82.51%
	F1-score	81.94%	83.96%	83.39%	85.62%

to classify the fused EDA+music feature vector. Without any attention module, the shallow feature extraction is abandoned and the RFE directly processes 3-channel EDA inputs. From Table 8, we can see although *Base* gets the poorest accuracy but the precision reaches 93%. This means the residual extractor tends to output the feature vector representing the high emotion state and is not discriminative enough for low state situation. The higher recognition accuracies from R_a and R_b prove the effectiveness of individual attention subnet, compared with *Base* model. When combining all the two modules, we can observe that the joint use of channel and temporal relationships R_c produces further improvement. Reviewing the results in Table 7, it should be emphasized that both SCA and RTNA are indispensable because all the sequential methods outperform the basic backbone when adding the single attention submodule.

Moreover, we compare 3 different arrangement of the SCA and RTNA: sequential SCA-RTNA, sequential RTNA-SCA and parallel use. For parallel method, the shallow features were forwarded into two submodules equally and the parallel outputs were added, then applied with sigmoid normalization. From the results in Table 7, we can see that the sequential method performs better than parallel method. And the channel-temporal order achieves the best performance. In addition, the channel attention-first order can slightly improve the recognition accuracy and stability compared with temporal attention-first order. Hence, we design the attention module with the SCA-RTNA order.

5.3.4 Attention Visualization

Recently, researches in neural network interpretation have proposed some methods for qualitative analysis. One of the most popular method is visualizing the weight distribution in the regions of input to show which parts are more important for predictions. Gradient-weighted Class Activation Mapping (Grad-CAM) [75] is an excellent visualization method which applies back gradient computing to reversely acquire the important weight of the input positions in convolutional layers. In image domain, the output

mask of Grad-CAM is overlaid on the semitransparent input image in the form of heatmap with a warm-to-cool color spectrum. As warmer color is applied, the highlighted pixels contribute more to the final prediction and the model will focus more on these messages. For different model, if the Grad-CAM mask covers more target regions in the same input, the receptive field of network is larger. And generally, it means the network has superior representation ability.

In order to show the ability of our attention submodules intuitively, we compare the visualization attention weights of the 3 trained model in the preceding experiment of Section 5.3.3: R_a (channel attention model), R_b (temporal attention model) and R_c (integrated channel-temporal attention model). To fit with the proposed framework, We adapt Grad-CAM and start the guided backpropagation from the output layer of each attention submodule to reversely acquire 1D attention weights in the 3-channel EDA input.

Fig. 5 and Fig. 7 show the sequences of preprocessed input signal and output attention weights from Grad-CAM. The input of valence and arousal situation (Subject-ID: 100184, Music-ID: 1) are randomly selected. In order to illustrate the corresponding relationship more clearly, the curves of 3-channel signal and the histogram of attention weights are displayed in one chart. Moreover, attention weights are presented in the form of spectrograms in Fig. 6 and Fig. 8. We can see that the attention weights of the channel attention module considers the relationships between different channels. The attention weights of the temporal attention module pay more attention to the temporal distribution. The attention weights of the integrated channel-temporal attention model selectively cover the regions better than other models because the corresponding spectrogram contains most warm color and black columns in chart are densest in important regions. It is also clear that the integrated RTCAN-1D pay more attention to the sharp peaks in 3 curves.

The quantitative experiment results in Section 5.3.3 and the qualitative visualization comparisons in this subsection can prove that the channel and temporal attention modules guide the proposed RTCAN-1D to improve the network's performance.

5.4 Comparison with previous methods

To validate the superiority of our proposed network, we provide extensive comparisons with the state-of-the-arts in three multimodal emotion datasets: DEAP, AMIGOS and large scale PMEmo. Those state-of-the-arts include both the handcrafted feature based conventional classifiers and deep learning based frameworks.

For single EDA input, previous works applied Support Vector Machine (SVM) [11], [12], Multi-Layer Perceptron (MLP) [77] and CNN based methods [62], [76], [78], [79] to classify the hand-craft features. We notice that the EDA decomposition is gradually being used for emotion recognition task [77], [78]. And after our previous work published [62], Ganapathy [78] also combined the CvxEDA and CNN model for EDA recognition. It should be noted that there are not many EDA-based emotion recognition in previous works, for example, there is no baseline using EDA signals for valence and arousal classification in

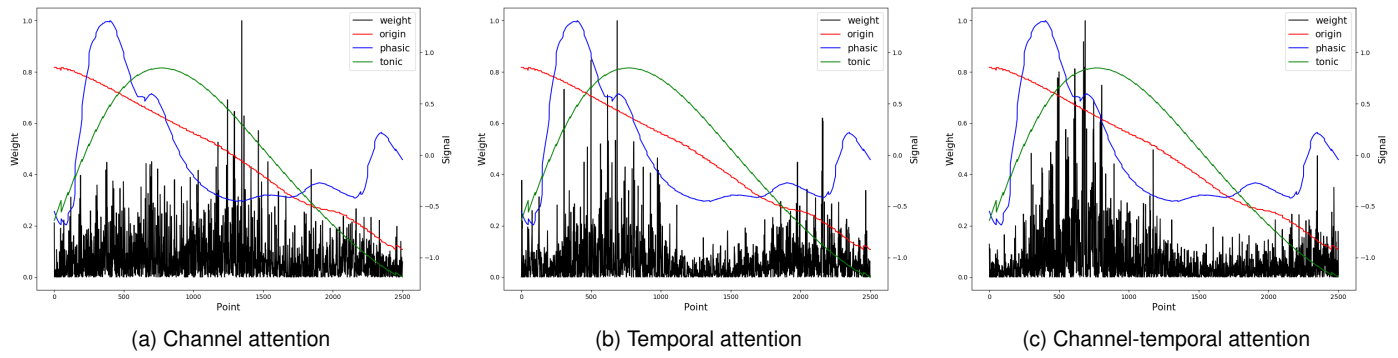


Fig. 5. The visualization of the curves of three signals and the column of attention weight in valence recognition with random subject (Subject-ID: 100184, Music-ID: 1). The red, blue and green curves respectively note the origin, phasic and tonic signals. The black columns represent the attention weight inverse mapping from the output features of attention submodules to 3-channel input.

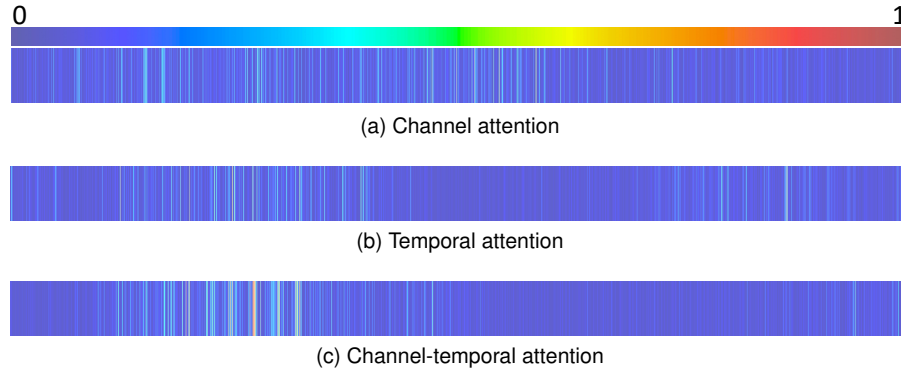


Fig. 6. The valence spectrogram visualization. The spectrograms in (a), (b), (c) are separately correspond to the attention weights in Fig. 5.

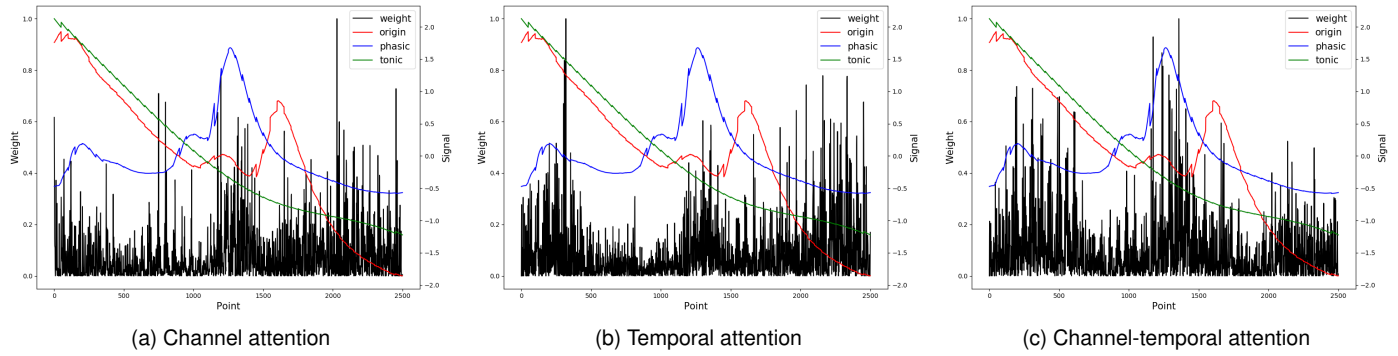


Fig. 7. The visualization of the curves of three signals and the column of attention weight in arousal recognition with random subject (Subject-ID: 100184, Music-ID: 1). The red, blue and green curves respectively note the origin, phasic and tonic signals. The black columns represent the attention weight inverse mapping from the output features of attention submodules to 3-channel input.

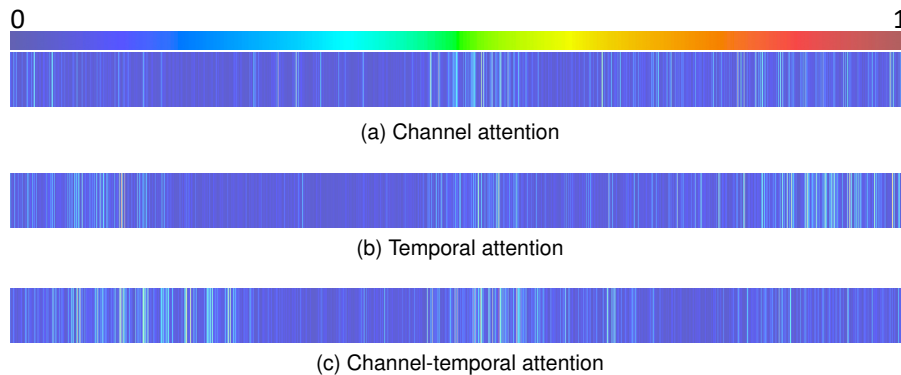


Fig. 8. The arousal spectrogram visualization. The spectrograms in (a), (b), (c) are separately correspond to the attention weights in Fig. 7.

TABLE 9
Comparison with previous works in AMIGOS, DEAP and PMEmo datasets.

Author	Dataset	Subjects	Signal	Model	Val	Ave-Accuracy	F1-Score
Correa <i>et la.</i> [12]	AMIGOS	40	EDA	SVM	10-fold	-	V: 52.80% A: 54.10%
Santamaria <i>et la.</i> [76]	AMIGOS	40	EDA	DCNN	-	V: 75.00% A: 71.00%	V: 71.00% A: 67.00%
Santamaria <i>et la.</i> [76]	AMIGOS	40	ECG+EDA	DCNN	-	V: 75.00% A: 76.00%	-
Our	AMIGOS	40	EDA	RTCAN-1D	10-fold	V: 74.13% A: 77.36%	V: 72.29% A: 76.46%
Koelstra <i>et la.</i> [11]	DEAP	32	EEG,EOG,EMG ,GSR,TMP,BVP,RSP	SVM	10-fold	V: 62.70% A: 57.00%	-
Sharma <i>et la.</i> [77]	DEAP	32	EDA	MLP	10-fold	V: 69.80% A: 79.00%	-
Ganapathy <i>et la.</i> [78]	DEAP	32	EDA	CNN	10-fold	V: 72.00% A: 75.00%	V: 71.41% A: 79.30%
Our	DEAP	32	EDA	RTCAN-1D	10-fold	V: 73.21% A: 81.05%	V: 77.37% A: 83.01%
Lin <i>et la.</i> [79]	DEAP	32	EEG,EOG,EMG ,GSR,TMP,BVP,RSP	Alexnet-2D	10-fold	V: 87.30% A: 85.50%	V: 78.24% A: 80.06%
Yin <i>et la.</i> [62]	PMEmo	457	EDA	Res-SIN	10-fold	V: 55.92% A: 57.24%	V: 58.83% A: 60.12%
Our	PMEmo	457	EDA	RTCAN-1D	10-fold	V: 57.83% A: 60.37%	V: 60.79% A: 63.15%
Yin <i>et la.</i> [62]	PMEmo	457	EDA+music	Res-SIN	10-fold	V: 73.43% A: 73.65%	V: 77.54% A: 78.56%
Our	PMEmo	457	EDA+music	RTCAN-1D	10-fold	V: 76.28% A: 82.05%	V: 80.09% A: 85.14%

DEAP dataset. Hence, for comprehensive evaluation, the comparisons are not limited in the EDA-based model. Other multimodal psychological signal-based methods (EEG,ECG) make use of traditional classifiers (*e.g.* KNN [80]) and deep learning model (*e.g.* DCNN [79], [81]).

Table 9 lists the comparisons between our model and previous studies. For binary recognition in DEAP, the evaluation results of our model are a little lower than the multi-physiological signals mixed method. It indicates the limitation of the single EDA input and the superiority of multi-feature fusion because the mixed input contains more affective messages than single input. But we still firmly believe the EDA-based emotion recognition is important and meaningful to the future user friendly applications for the reliability and easy-acquisition of EDA signal. The results in all three datasets validate the superiority of our RTCAN-1D.

6 CONCLUSION

In this work, we propose an end-to-end framework named 1-dimensional residual temporal and channel attention network (RTCAN-1D) for EDA-based user independent emotion recognition. In conclusion, the great performance of the proposed RTCAN-1D attributes to: (1) the novel decomposition of CvxEDA to directly acquire the steady and dynamic activity from raw EDA; (2) the temporal-channel attention modules to mine the long-range temporal correlations and channel-wise relationships to reweight the distribution of the shallow features; (3) the fusion of emotion benchmarks from external stimulation and the individual specificity from EDA for large scale participant dataset. The extensive experiments in three popular datasets show an excellent generalization ability and validate the superiority of our model. In future work, the fusion of external static features

and traditional physiological signals will be an efficient way for large scale affective computing. The attention mechanism can also further improve the ability of CNN-based end-to-end frameworks. We believe the research of EDA-based emotion recognition will promote a lot of practical applications.

ACKNOWLEDGMENT

This research work is supported by the Key Project of National Science Foundation of Zhe-jiang Province (No. LZ19F020002). And the authors would like to thank the Key Laboratory of Design Intelligence and Digital Creativity of Zhejiang Province, Alibaba-Zhejiang University Joint Institute of Frontier Technologies.

REFERENCES

- [1] R. W. Picard, *Affective computing*. MIT press, 2000.
- [2] R. Guo, S. Li, L. He, W. Gao, H. Qi, and G. Owens, "Pervasive and unobtrusive emotion sensing for human mental health," in *2013 7th International Conference on Pervasive Computing Technologies for Healthcare and Workshops*. IEEE, 2013, pp. 436–439.
- [3] C. D. Katsis, N. Katertsidis, G. Ganiatsas, and D. I. Fotiadis, "Toward emotion recognition in car-racing drivers: A biosignal processing approach," *IEEE Transactions on Systems, Man, and Cybernetics-Part A: Systems and Humans*, vol. 38, no. 3, pp. 502–512, 2008.
- [4] A. Sano and R. W. Picard, "Stress recognition using wearable sensors and mobile phones," in *2013 Humaine Association Conference on Affective Computing and Intelligent Interaction*. IEEE, 2013, pp. 671–676.
- [5] R. W. Picard, E. Vyzas, and J. Healey, "Toward machine emotional intelligence: Analysis of affective physiological state," *IEEE Transactions on Pattern Analysis & Machine Intelligence*, no. 10, pp. 1175–1191, 2001.
- [6] P. Ekman, "An argument for basic emotions," *Cognition & emotion*, vol. 6, no. 3-4, pp. 169–200, 1992.

- [7] C. L. Stephens, I. C. Christie, and B. H. Friedman, "Autonomic specificity of basic emotions: Evidence from pattern classification and cluster analysis," *Biological psychology*, vol. 84, no. 3, pp. 463–473, 2010.
- [8] S. Hamann, "Mapping discrete and dimensional emotions onto the brain: controversies and consensus," *Trends in cognitive sciences*, vol. 16, no. 9, pp. 458–466, 2012.
- [9] J. A. Russell, "A circumplex model of affect," *Journal of personality and social psychology*, vol. 39, no. 6, p. 1161, 1980.
- [10] P. J. Lang, M. K. Greenwald, M. M. Bradley, and A. O. Hamm, "Looking at pictures: Affective, facial, visceral, and behavioral reactions," *Psychophysiology*, vol. 30, no. 3, pp. 261–273, 1993.
- [11] S. Koelstra, C. Muhl, M. Soleymani, J.-S. Lee, A. Yazdani, T. Ebrahimi, T. Pun, A. Nijholt, and I. Patras, "Deap: A database for emotion analysis; using physiological signals," *IEEE transactions on affective computing*, vol. 3, no. 1, pp. 18–31, 2011.
- [12] J. A. M. Correa, M. K. Abadi, N. Sebe, and I. Patras, "Amigos: a dataset for affect, personality and mood research on individuals and groups," *IEEE Transactions on Affective Computing*, 2018.
- [13] K. Zhang, H. Zhang, S. Li, C. Yang, and L. Sun, "The pmemo dataset for music emotion recognition," in *Proceedings of the 2018 ACM on International Conference on Multimedia Retrieval*. ACM, 2018, pp. 135–142.
- [14] R. Adolphs, D. Tranel, S. Hamann, A. W. Young, A. J. Calder, E. A. Phelps, A. Anderson, G. P. Lee, and A. R. Damasio, "Recognition of facial emotion in nine individuals with bilateral amygdala damage," *Neuropsychologia*, vol. 37, no. 10, pp. 1111–1117, 1999.
- [15] M. El Ayadi, M. S. Kamel, and F. Karray, "Survey on speech emotion recognition: Features, classification schemes, and databases," *Pattern Recognition*, vol. 44, no. 3, pp. 572–587, 2011.
- [16] S. Jerritta, M. Murugappan, R. Nagarajan, and K. Wan, "Physiological signals based human emotion recognition: a review," in *2011 IEEE 7th International Colloquium on Signal Processing and its Applications*. IEEE, 2011, pp. 410–415.
- [17] J. Shukla, M. Barreda-Angeles, J. Oliver, G. Nandi, and D. Puig, "Feature extraction and selection for emotion recognition from electrodermal activity," *IEEE Transactions on Affective Computing*, 2019.
- [18] M. D. van der Zwaag, J. H. Janssen, and J. H. Westerink, "Directing physiology and mood through music: Validation of an affective music player," *IEEE Transactions on Affective Computing*, vol. 4, no. 1, pp. 57–68, 2012.
- [19] J. Wang and Y. Gong, "Recognition of multiple drivers emotional state," in *2008 19th International Conference on Pattern Recognition*. IEEE, 2008, pp. 1–4.
- [20] J. Healey, R. W. Picard *et al.*, "Detecting stress during real-world driving tasks using physiological sensors," *IEEE Transactions on intelligent transportation systems*, vol. 6, no. 2, pp. 156–166, 2005.
- [21] M. Swangnetr and D. B. Kaber, "Emotional state classification in patient-robot interaction using wavelet analysis and statistics-based feature selection," *IEEE Transactions on Human-Machine Systems*, vol. 43, no. 1, pp. 63–75, 2012.
- [22] J. Shukla, M. Barreda-Ángeles, J. Oliver, and D. Puig, "Efficient wavelet-based artifact removal for electrodermal activity in real-world applications," *Biomedical Signal Processing and Control*, vol. 42, pp. 45–52, 2018.
- [23] S. Jirayucharoensak, S. Pan-Ngum, and P. Israsena, "Eeg-based emotion recognition using deep learning network with principal component based covariate shift adaptation," *The Scientific World Journal*, vol. 2014, 2014.
- [24] P. Bashivan, I. Rish, M. Yeasin, and N. Codella, "Learning representations from eeg with deep recurrent-convolutional neural networks," *arXiv preprint arXiv:1511.06448*, 2015.
- [25] R. T. Schirmmeister, J. T. Springenberg, L. D. J. Fiederer, M. Glasstetter, K. Eggenberger, M. Tangermann, F. Hutter, W. Burgard, and T. Ball, "Deep learning with convolutional neural networks for eeg decoding and visualization," *Human brain mapping*, vol. 38, no. 11, pp. 5391–5420, 2017.
- [26] G. Keren, T. Kirschstein, E. Marchi, F. Ringeval, and B. Schuller, "End-to-end learning for dimensional emotion recognition from physiological signals," in *2017 IEEE International Conference on Multimedia and Expo (ICME)*, 2017, pp. 985–990.
- [27] J. Kim and E. André, "Emotion recognition based on physiological changes in music listening," *IEEE transactions on pattern analysis and machine intelligence*, vol. 30, no. 12, pp. 2067–2083, 2008.
- [28] C. Maaoui and A. Pruski, "Emotion recognition through physiological signals for human-machine communication," in *Cutting Edge Robotics 2010*. IntechOpen, 2010.
- [29] Y.-H. Yang and H. H. Chen, *Music emotion recognition*. CRC Press, 2011.
- [30] A. Hanjalic and L.-Q. Xu, "Affective video content representation and modeling," *IEEE transactions on multimedia*, vol. 7, no. 1, pp. 143–154, 2005.
- [31] C. A. Torres, Á. A. Orozco, and M. A. Álvarez, "Feature selection for multimodal emotion recognition in the arousal-valence space," in *2013 35th Annual International Conference of the IEEE Engineering in Medicine and Biology Society (EMBC)*. IEEE, 2013, pp. 4330–4333.
- [32] A. Greco, G. Valenza, A. Lanata, E. P. Scilingo, and L. Citi, "cvxeda: A convex optimization approach to electrodermal activity processing," *IEEE Transactions on Biomedical Engineering*, vol. 63, no. 4, pp. 797–804, 2015.
- [33] R. Plutchik, "A psychoevolutionary theory of emotions," *Social Science Information*, vol. 21, pp. 529–553, 1982.
- [34] A. R. Damasio, *Descartes' Error: Emotion, Reason, and the Human Brain*, 1994.
- [35] C. E. Izard, "Basic emotions, natural kinds, emotion schemas, and a new paradigm," *Perspectives on Psychological Science*, vol. 2, no. 3, pp. 260–280, 2007.
- [36] W. M. Wundt, "Vorlesungen ber die menschen- und tierseele," *American Journal of Psychology*, vol. 32, no. 1, p. 151, 1921.
- [37] M. E. Dawson, A. M. Schell, and D. L. Filion, "The electrodermal system," *Handbook of psychophysiology*, vol. 2, pp. 200–223, 2007.
- [38] M. Soleymani, J. Lichtenauer, T. Pun, and M. Pantic, "A multi-modal database for affect recognition and implicit tagging," *IEEE Transactions on Affective Computing*, vol. 3, no. 1, pp. 42–55, 2011.
- [39] T. Baltrušaitis, C. Ahuja, and L.-P. Morency, "Multimodal machine learning: A survey and taxonomy," *IEEE transactions on pattern analysis and machine intelligence*, vol. 41, no. 2, pp. 423–443, 2018.
- [40] N. Xiong and P. Svensson, "Multi-sensor management for information fusion: issues and approaches," *Information fusion*, vol. 3, no. 2, pp. 163–186, 2002.
- [41] A. Jaimes and N. Sebe, "Multimodal human-computer interaction: A survey," *Computer vision and image understanding*, vol. 108, no. 1–2, pp. 116–134, 2007.
- [42] K. H. Kim, S. W. Bang, and S. R. Kim, "Emotion recognition system using short-term monitoring of physiological signals," *Medical and biological engineering and computing*, vol. 42, no. 3, pp. 419–427, 2004.
- [43] J. Kim, "Bimodal emotion recognition using speech and physiological changes," *Robust speech recognition and understanding*, vol. 265, p. 280, 2007.
- [44] J. Liu, Y. Su, and Y. Liu, "Multi-modal emotion recognition with temporal-band attention based on lstm-rnn," in *Pacific Rim Conference on Multimedia*. Springer, 2017, pp. 194–204.
- [45] S. Koelstra and I. Patras, "Fusion of facial expressions and eeg for implicit affective tagging," *Image and Vision Computing*, vol. 31, no. 2, pp. 164–174, 2013.
- [46] N. Thammasan, K.-i. Fukui, and M. Numao, "Multimodal fusion of eeg and musical features in music-emotion recognition," in *Thirty-First AAAI Conference on Artificial Intelligence*, 2017.
- [47] A. Gelman, "A bayesian formulation of exploratory data analysis and goodness-of-fit testing," *International Statistical Review*, vol. 71, no. 2, pp. 369–382, 2007.
- [48] M. Kelsey, A. Dallal, S. Eldeeb, M. Akcakaya, I. Kleckner, C. Gerard, K. S. Quigley, and M. S. Goodwin, "Dictionary learning and sparse recovery for electrodermal activity analysis," in *Compressive Sensing V: From Diverse Modalities to Big Data Analytics*, vol. 9857, 2016.
- [49] M. Kelsey, M. Akcakaya, I. R. Kleckner, R. V. Palumbo, L. F. Barrett, K. S. Quigley, and M. S. Goodwin, "Applications of sparse recovery and dictionary learning to enhance analysis of ambulatory electrodermal activity data," *Biomedical Signal Processing and Control*, vol. 40, pp. 58–70, 2018.
- [50] D. M. Alexander, C. Trengove, P. Johnston, T. Cooper, J. August, and E. Gordon, "Separating individual skin conductance responses in a short interstimulus-interval paradigm," *Journal of neuroscience methods*, vol. 146, no. 1, pp. 116–123, 2005.
- [51] W. Boucsein, *Electrodermal activity*. Springer Science & Business Media, 2012.
- [52] M. Benedek and C. Kaernbach, "Decomposition of skin conductance data by means of nonnegative deconvolution," *Psychophysiology*, vol. 47, no. 4, pp. 647–658, 2010.

- [53] —, “A continuous measure of phasic electrodermal activity,” *Journal of neuroscience methods*, vol. 190, no. 1, pp. 80–91, 2010.
- [54] A. Greco, G. Valenza, L. Citi, and E. P. Scilingo, “Arousal and valence recognition of affective sounds based on electrodermal activity,” *IEEE Sensors Journal*, vol. 17, no. 3, pp. 716–725, 2016.
- [55] J. Hu, L. Shen, and G. Sun, “Squeeze-and-excitation networks,” in *Proceedings of the IEEE conference on computer vision and pattern recognition*, 2018, pp. 7132–7141.
- [56] X. Wang, R. Girshick, A. Gupta, and K. He, “Non-local neural networks,” in *Proceedings of the IEEE Conference on Computer Vision and Pattern Recognition*, 2018, pp. 7794–7803.
- [57] A. Vaswani, N. Shazeer, N. Parmar, J. Uszkoreit, L. Jones, A. N. Gomez, L. Kaiser, and I. Polosukhin, “Attention is all you need,” in *Advances in neural information processing systems*, 2017, pp. 5998–6008.
- [58] W. Pei, T. Baltrusaitis, D. M. Tax, and L.-P. Morency, “Temporal attention-gated model for robust sequence classification,” in *Proceedings of the IEEE Conference on Computer Vision and Pattern Recognition*, 2017, pp. 6730–6739.
- [59] D. Yu and L. Deng, “Deep learning and its applications to signal and information processing [exploratory dsp],” *IEEE Signal Processing Magazine*, vol. 28, no. 1, pp. 145–154, 2010.
- [60] S.-Y. Chang and N. Morgan, “Robust cnn-based speech recognition with gabor filter kernels,” in *Fifteenth annual conference of the international speech communication association*, 2014.
- [61] K. He, X. Zhang, S. Ren, and J. Sun, “Deep residual learning for image recognition,” in *Proceedings of the IEEE conference on computer vision and pattern recognition*, 2016, pp. 770–778.
- [62] G. Yin, S. Sun, H. Zhang, D. Yu, C. Li, K. Zhang, and N. Zou, “User independent emotion recognition with residual signal-image network,” in *2019 IEEE International Conference on Image Processing (ICIP)*. IEEE, 2019, pp. 3277–3281.
- [63] K. Simonyan and A. Zisserman, “Very deep convolutional networks for large-scale image recognition,” *arXiv preprint arXiv:1409.1556*, 2014.
- [64] C. Szegedy, W. Liu, Y. Jia, P. Sermanet, S. Reed, D. Anguelov, D. Erhan, V. Vanhoucke, and A. Rabinovich, “Going deeper with convolutions,” in *Proceedings of the IEEE conference on computer vision and pattern recognition*, 2015, pp. 1–9.
- [65] G. Huang, Z. Liu, L. Van Der Maaten, and K. Q. Weinberger, “Densely connected convolutional networks,” in *Proceedings of the IEEE conference on computer vision and pattern recognition*, 2017, pp. 4700–4708.
- [66] L. Chen, H. Zhang, J. Xiao, L. Nie, J. Shao, W. Liu, and T.-S. Chua, “Sca-cnn: Spatial and channel-wise attention in convolutional networks for image captioning,” in *Proceedings of the IEEE conference on computer vision and pattern recognition*, 2017, pp. 5659–5667.
- [67] S. Woo, J. Park, J.-Y. Lee, and I. So Kweon, “Cbam: Convolutional block attention module,” in *Proceedings of the European Conference on Computer Vision (ECCV)*, 2018, pp. 3–19.
- [68] A. Buades, B. Coll, and J.-M. Morel, “A non-local algorithm for image denoising,” in *2005 IEEE Computer Society Conference on Computer Vision and Pattern Recognition (CVPR’05)*, vol. 2. IEEE, 2005, pp. 60–65.
- [69] C. A. Frantzidis, C. Bratsas, M. A. Klados, E. Konstantinidis, C. D. Lithari, A. B. Vivas, C. L. Papadelis, E. Kaldoudi, C. Pappas, and P. D. Bamidis, “On the classification of emotional biosignals evoked while viewing affective pictures: an integrated data-mining-based approach for healthcare applications,” *IEEE Transactions on Information Technology in Biomedicine*, vol. 14, no. 2, pp. 309–318, 2010.
- [70] Z. Yin, Y. Wang, L. Liu, W. Zhang, and J. Zhang, “Cross-subject eeg feature selection for emotion recognition using transfer recursive feature elimination,” *Frontiers in neurorobotics*, vol. 11, p. 19, 2017.
- [71] N. Ganapathy, Y. R. Veeranki, and R. Swaminathan, “Convolutional neural network based emotion classification using electrodermal activity signals and time-frequency features,” *Expert Systems with Applications*, p. 113571, 2020.
- [72] H. Ferdinando and E. Alasaarela, “Emotion recognition using cvxeda-based features,” *Journal of Telecommunication, Electronic and Computer Engineering (JTEC)*, vol. 10, no. 2-3, pp. 19–23, 2018.
- [73] A. Aljanaki, Y.-H. Yang, and M. Soleymani, “Developing a benchmark for emotional analysis of music,” *PloS one*, vol. 12, no. 3, p. e0173392, 2017.
- [74] K. He and J. Sun, “Convolutional neural networks at constrained time cost,” in *Proceedings of the IEEE conference on computer vision and pattern recognition*, 2015, pp. 5353–5360.
- [75] R. R. Selvaraju, M. Cogswell, A. Das, R. Vedantam, D. Parikh, and D. Batra, “Grad-cam: Visual explanations from deep networks via gradient-based localization,” in *Proceedings of the IEEE International Conference on Computer Vision*, 2017, pp. 618–626.
- [76] L. Santamaria-Granados, M. Munoz-Organero, G. Ramirez-Gonzalez, E. Abdulhay, and N. Arunkumar, “Using deep convolutional neural network for emotion detection on a physiological signals dataset (amigos),” *IEEE Access*, vol. 7, pp. 57–67, 2018.
- [77] V. Sharma, N. R. Prakash, and P. Kalra, “Audio-video emotional response mapping based upon electrodermal activity,” *Biomedical Signal Processing and Control*, vol. 47, pp. 324 – 333, 2019.
- [78] N. Ganapathy, Y. R. Veeranki, and R. Swaminathan, “Convolutional neural network based emotion classification using electrodermal activity signals and time-frequency features,” *Expert Systems with Applications*, vol. 159, p. 113571, 2020.
- [79] W. Lin, C. Li, and S. Sun, “Deep convolutional neural network for emotion recognition using eeg and peripheral physiological signal,” in *International Conference on Image and Graphics*. Springer, 2017, pp. 385–394.
- [80] J. Liu, H. Meng, A. Nandi, and M. Li, “Emotion detection from eeg recordings,” in *2016 12th International Conference on Natural Computation, Fuzzy Systems and Knowledge Discovery (ICNC-FSKD)*. IEEE, 2016, pp. 1722–1727.
- [81] P. Sarkar and A. Etemad, “Self-supervised learning for eeg-based emotion recognition,” *arXiv preprint arXiv:1910.07497*, 2019.